



**POLITECNICO**  
MILANO 1863

DIPARTIMENTO DI MECCANICA



## Domain-selective functional analysis of variance for supervised statistical profile monitoring of signal data

Pini, Alessia; Vantini, Simone; Colosimo, BIANCA MARIA; Grasso, MARCO LUIGI

This is the peer reviewed version of the following article: Pini, A., Vantini, S., Colosimo, B.M. and Grasso, M. (2018), Domain-selective functional analysis of variance for supervised statistical profile monitoring of signal data. J. R. Stat. Soc. C, 67: 55-81, which has been published in final form at <https://doi.org/10.1111/rssc.12218>. This article may be used for non-commercial purposes in accordance with Wiley Terms and Conditions for Use of Self-Archived Versions.

This content is provided under [CC BY-NC-ND 4.0](#) license



# Domain-Selective Functional ANOVA for Supervised Statistical Profile Monitoring of Signal Data

Alessia Pini, Simone Vantini

MOX - Department of Mathematics, Politecnico di Milano, Milano, Italy

alessia.pini@polimi.it, simone.vantini@polimi.it

and

Bianca Maria Colosimo and Marco Grasso

Department of Mechanical Engineering, Politecnico di Milano, Milano, Italy

biancamaria.colosimo@polimi.it, marcoluigi.grasso@polimi.it

## Abstract

In many applications, process monitoring has to deal with functional responses, also known as profile data. In these scenarios, a relevant industrial problem consists of detecting faults by combining supervised learning to functional data analysis and statistical process monitoring. Supervised learning is usually applied to the whole signal domain, with the aim of discovering the features that are affected by the faults of interest. In this paper we explore a different perspective, which consists of performing supervised learning to inferentially select the parts of the signal data that are more informative in terms of underlying fault factors. The procedure is based on a non-parametric domain-selective functional ANOVA and allows to identify the specific subintervals where the profile is sensitive to process changes. Benefits achieved by coupling the proposed approach with profile monitoring are highlighted using a simulation study. We show how applying profile monitoring only to the identified subintervals can reduce the time to detect the out-of-control state of the process. To illustrate its potentiality in industrial applications, the proposed procedure is applied to remote laser welding, where the main aim is monitoring the gap between the welded plates through the observation of the emission spectra of the welded material.

*Keywords:* Design of Experiments, Interval-Wise Error Rate, Functional Data Analysis, Statistical Process Control

# 1 Introduction

The continuous technological advances of in-situ sensing systems and non-contact data acquisition architectures allow gathering a huge amount of information about the process in every operating condition. In particular, more and more often responses of manufacturing processes can be modeled as functional data, i.e., a vector of data, where each value corresponds to a specific temporal or spatial location.

Functional data can in fact represent the shape of a machined feature and/or the pattern of a signal acquired during the process over time. In this scenario, statistical quality monitoring (also known as statistical process control, SPC) has to be appropriately rethought to deal with functional responses. With reference to statistical quality monitoring, the problem of checking the stability of a functional response has been named “profile monitoring” and has attracted the attention of many researchers over the past ten years (for an overview, see, for instance, Noorossana et al. 2012 and references therein). It consists of detecting a change of the functional response pattern that is deemed to be due to an out-of-control state of the manufacturing process.

Traditional approaches for profile monitoring are designed considering an “unsupervised” mode. In this case, a set of in-control profiles are used in the design phase (usually referred to as Phase I in SPC literature), as the monitoring strategy consists of detecting any kind of change from the in-control state by issuing an alarm. However, in many industrial problems, faults have not the same impact on the process performance, and changes from the in-control state can be of various nature. Supervised approaches should be preferred instead, where the term “supervised” refers to the use of out-of-control information in the control chart design phase. [Indeed, thanks to continuous advances of sensing technologies and data acquisition networks, a huge amount of information about the industrial process is potentially available. This enables a better comprehension of process dynamics that yields a deeper knowledge of every process state, including fault onset phenomena. The underlying idea of so-called supervised monitoring consists of exploiting this knowledge since the control chart design stage.](#) Different authors (Basseville, 1988; Box and Ramirez, 1992; Runger and Testik, 2003) pointed out that incorporating a priori knowledge of a fault signature, when available, into control chart design is suitable to develop fault-sensitized SPC schemes, possibly used in combination with traditional control charts. As far as univariate processes are concerned, two methods were proposed to this aim, one based on Cuscore charts (Box and Ramirez, 1992; Shu et al., 2002; Nembhard, 2006; Box and Luceno, 2011) and one based on the generalized likelihood ratio statistic (Lorden, 1971; Lai, 1995). A comparison between the two methods were discussed by Runger and Testik (2003). Recently, the studies of Zhang et al. (2014, 2015) extended this concept to profile

monitoring applications. Specifically, Zhang et al. (2014, 2015) studied profile monitoring schemes for linear profiles where the out-of-control departure is known in advance and it consists of a shape change from a straight line to a second-order polynomial curve. The underlying idea was to develop control charting schemes based on testing the significance of the quadratic term.

Our study extends that method by considering non-linear profiles of general shape, where a functional basis expansion is used to approximate the profile pattern. As a matter of fact, in many industrial applications, the process change does not affect a single term of the basis expansion, but it influences a portion of the profile domain. Thus, a fault-sensitized control chart can be developed by monitoring only that relevant portion, with several benefits including dimensional reduction and faster detection of known faults. This kind of control chart can possibly be used to supplement traditional charts, by combining general purpose (unsupervised) and fault-sensitized (supervised) monitoring tools (Runger and Testik, 2003). In a production environment, such a control chart can be designed either for faults that are more likely to occur or for out-of-control conditions whose high criticality implies the need to make the detection as fast as possible.

To efficiently and effectively monitor the process, it is then necessary to develop reliable methods to select informative parts of the functional pattern. Even though such a selection can be done in qualitative ways, for instance by a visual inspection of the data, or based on engineering knowledge about the process, in some cases visual inspection and/or prior knowledge can be unclear, and may neglect important aspects. Hence, we here propose a quantitative statistical technique for domain selection. The approach that we propose is sound even in absence of full prior knowledge about the process, and it is expected to yield clearer and more reliable results. We propose to select the informative parts of the functions by means of the inferential interval-wise testing procedure, first proposed in Pini and Vantini (2015), and extended here to the case of multi-way functional ANOVA. In detail, we test the significance of the effects of the factors on the output functions when process changes can be experimentally observed, e.g. by injecting faults into the system during an exploratory phase that precedes the control chart design. More importantly, we provide a selection of the parts of the domain presenting significant effects of each factor. Once this selection has been done, we propose to monitor the industrial process based on the information that the functions contain on the selected domains. A simulation study is presented to quantify the benefits resulting from coupling the interval-wise testing procedure with profile monitoring techniques. In addition, a real case study is discussed, which consists of a remote laser welding operation, where a laser emission spectrum is used as a reference to check whether the distance between the plates to be welded (i.e., the gap) is appropriate. In this case, a previous study (Colombo et al., 2013) showed that the gap

between the plates affects the emission spectra and it can be used for monitoring purposes. Moreover, developing a specific sensor aimed at detecting the emission just at some specific wavelength instead of using the whole spectra can reduce the costs of the monitoring device and reduce the computational time.

The paper is structured as follows: Section 2 presents the statistical methodology. Section 3 presents the simulation study that includes a comparison between competitor methods for profile monitoring. Section 4 reports an application of the proposed method on a remote laser welding data set. Section 5 concludes the paper. A robustness analysis is reported in the Appendix. All computations and plots have been created using R (R Core Team, 2012).

## 2 The proposed methodology

The proposed methodology extends the traditional control chart design phase by including a preliminary experimental step aimed at identifying the domain of the functional pattern affected by the process. Thus, two sequential steps are required. First, a fault-driven design of experiments is performed by injecting faults into the system. An analysis of variance (ANOVA) is carried out to study the effects of these faults on the functional signal pattern. In some cases, small-scale test benches or computer experiments can be used to this aim when a direct fault analysis on the full scale plant is not viable. The kind of analysis we propose to perform in this step is a domain-selective functional ANOVA based on interval-wise testing.

During the second step, such knowledge is used to drive, in a supervised way, the design of a profile monitoring tool, where only the selected portion of the functional pattern is taken into account. In the following, the two building blocks of the proposed methodology are presented. Subsection 2.1 presents the domain-selective functional ANOVA methodology, whereas the development of supervised profile monitoring is discussed in Subsection 2.2.

### 2.1 Domain-selective functional ANOVA

Aim of this section is to describe the interval-wise testing methodology to select statistically relevant portions of the functional pattern, and to extend it to a multi-way ANOVA design. For ease of notation, and without loss of generality, we consider the example of a two-way functional ANOVA with an interaction. Nevertheless, the methodology presented here can be directly generalized to the analysis of factorial design with more than two factors.

Consider a two-way ANOVA in which we investigate the effects of factors  $A$  and  $B$  (with

$I$  and  $J$  levels, respectively) on a functional response based on a replicated full factorial design. We assume that the response of the model is a function of a continuous variable  $t$  observed over a domain  $(a, b) \subset \mathbb{R}$ . In the considered model, the functional response will be expressed as the result of two main effects, and of an interaction between them. The aim of the analysis is to test the significance of every term in the model (i.e., interaction and main effects).

In detail, let  $y_{ijl} : (a, b) \mapsto \mathbb{R}$  be the output functional data, where  $i$  denotes the level of the first factor,  $j$  denotes the level of the second factor, and  $l$  denotes the replicate. We assume functional data to be continuous functions of the variable  $t$ . Note that, as shown in Pini and Vantini (2015), this condition can be relaxed, and the methodology can be applied to generic  $L^2$  functions. The functional ANOVA model that we want to test is thus the following:

$$y_{ijl}(t) = \mu(t) + \alpha_i(t) + \beta_j(t) + \gamma_{ij}(t) + \epsilon_{ijl}(t), \quad (1)$$

where  $t \in (a, b)$ , with  $i = 1, \dots, I$ ,  $j = 1, \dots, J$ ,  $l = 1, \dots, n_{ij}$ ,  $n_{ij}$  being the number of replicates for  $i^{\text{th}}$  level of the first factor and  $j^{\text{th}}$  level of the second factor. In model (1),  $\mu(t)$  is the functional grand mean,  $\alpha_i(t)$  and  $\beta_j(t)$  are functional main effects, and  $\gamma_{ij}(t)$  is the functional interaction effect. The functional errors  $\epsilon_{ijl}(t)$  are assumed to be independent and identically distributed zero-mean random functions. Note that the proposed technique can deal with autocorrelated functional data since we only require independence between units, and not between time instants. Furthermore, we do not require the errors to follow a gaussian process. All effects (as well as the errors) are expressed as functions of the continuous variable  $t$ . For sake of identifiability, we require the classical constraints on the effects, i.e.,  $\forall t \in (a, b)$ :  $\sum_{i=1}^I n_{i\cdot} \alpha_i(t) = 0$ ;  $\sum_{j=1}^J n_{\cdot j} \beta_j(t) = 0$ ;  $\sum_{i=1}^I \sum_{j=1}^J n_{ij} \gamma_{ij}(t) = 0$ , where  $n_{i\cdot} = \sum_{j=1}^J n_{ij}$  denotes the number of units at  $i^{\text{th}}$  level of the first factor and  $n_{\cdot j} = \sum_{i=1}^I n_{ij}$  denotes the number of units at  $j^{\text{th}}$  level of the second factor.

The aim of our analysis is to test the significance of all coefficients of model (1). In particular, we want to perform the functional counterparts of uni/multivariate ANOVA tests:

- a functional test of the null model, jointly for all factors:

$$\begin{cases} H_{0,Model} & : \alpha_i(t) = \beta_j(t) = \gamma_{ij}(t) = 0 \forall i = 1, \dots, I; j = 1, \dots, J; t \in (a, b); \\ H_{1,Model} & : (H_{0,Model})^C; \end{cases} \quad (2)$$

- three functional tests for the effects of each factor and interaction:

$$H_{0,A} : \alpha_i(t) = 0 \forall i = 1, \dots, I; t \in (a, b); \quad H_{1,A} : (H_{0,A})^C \quad (3)$$

$$H_{0,B} : \beta_j(t) = 0 \forall j = 1, \dots, J; t \in (a, b); \quad H_{1,B} : (H_{0,B})^C \quad (4)$$

$$H_{0,AB} : \gamma_{ij}(t) = 0 \forall i = 1, \dots, I; j = 1, \dots, J; t \in (a, b); \quad H_{1,AB} : (H_{0,AB})^C. \quad (5)$$

Note that, similarly to uni/multivariate two-way ANOVA, (2) is a test of significance of the whole functional model, whereas the three tests (3-5) allow performing a model selection. The main difference with respect to a uni/multivariate ANOVA is that the tests (2-5) involve functional coefficients, i.e., the null hypothesis is rejected whenever there is a significant difference between the corresponding groups in at least one interval of the domain.

The problem of inference in FDA has been widely discussed in the literature of the last decades, and it can be addressed in several ways (e.g., Cuevas et al., 2004; Abramovich and Angelini, 2006; Antoniadis and Sapatinas, 2007; Cuesta-Albertos and Febrero-Bande, 2010; Goldsmith and Kitago, 2016; Pomann et al., 2016). A common feature of all these works, is that the final result from the ANOVA testing determines whether the hypotheses (2-5) are globally accepted or rejected. In particular, by applying these tests, we are only able to answer the question “Are there any statistically significant effects of factors  $A$  and/or  $B$  on the functional responses?”. In the case of a positive answer, these tests are not able to select the intervals of the domain in which the effects are detected.

On the contrary, the principal aim of this paper is to provide practitioners with a methodology that selects the most informative parts of the functions domain, in order to use this information to design supervised monitoring tools. In detail, for each tests (2-5), in case of rejection of the null hypothesis, we want to select the intervals of the variable  $t$  where significant differences are detected. For this reason, we extend the interval-wise testing proposed in (Pini and Vantini, 2015), that is a testing procedure for functional data that enables to select the intervals of the domain presenting significant effects. Another advantage of this procedure is that it is not based on parametric assumptions. We neither need to assume normality of the residuals, nor to specify their covariance structure.

The extension of the procedure to functional ANOVA is based on three steps, detailed in the following paragraphs.

**First step: interval-wise testing.** A functional test corresponding to tests (2-5) is performed on any interval of the domain. In detail, [for every](#)  $\mathcal{I} \subseteq (a, b)$ , we perform a test

of the null model, and three tests on the main effects and interaction:

$$\begin{cases} H_{0,Model}^{\mathcal{I}} & : \alpha_i(t) = \beta_j(t) = \gamma_{ij}(t) = 0 \quad \forall i = 1, \dots, I; j = 1, \dots, J; t \in \mathcal{I}; \\ H_{1,Model}^{\mathcal{I}} & : (H_{0,Model}^{\mathcal{I}})^C \end{cases} \quad (6)$$

$$H_{0,A}^{\mathcal{I}} : \alpha_i(t) = 0 \quad \forall i = 1, \dots, I; t \in \mathcal{I}; \quad H_{1,A}^{\mathcal{I}} : (H_{0,A}^{\mathcal{I}})^C \quad (7)$$

$$H_{0,B}^{\mathcal{I}} : \beta_j(t) = 0 \quad \forall j = 1, \dots, J; t \in \mathcal{I}; \quad H_{1,B}^{\mathcal{I}} : (H_{0,B}^{\mathcal{I}})^C \quad (8)$$

$$H_{0,AB}^{\mathcal{I}} : \gamma_{ij}(t) = 0 \quad \forall i = 1, \dots, I; j = 1, \dots, J; t \in \mathcal{I}; \quad H_{1,AB}^{\mathcal{I}} : (H_{0,AB}^{\mathcal{I}})^C. \quad (9)$$

As proposed in Pini and Vantini (2015), we perform each test in a permutation framework. In detail, we apply permutations of the residuals of the reduced model according to the Freedman and Lane permutation scheme (Freedman and Lane, 1983). As common practice in the permutational framework, we use classical test statistics. In particular, we use the integral over the interval  $\mathcal{I}$  of the two-way ANOVA statistics of the corresponding classical  $F$ -tests.

In details, for the test of  $H_{0,Model}^{\mathcal{I}}$  we use:

$$F_{Model}^{\mathcal{I}} = \int_{\mathcal{I}} \frac{\sum_{i=1}^I \sum_{j=1}^J \sum_{l=1}^{n_{ij}} (\hat{y}_{ij}(t) - \bar{y}(t))^2 / df_{Model}}{\sum_{i=1}^I \sum_{j=1}^J \sum_{l=1}^{n_{ij}} (y_{ijl}(t) - \bar{y}(t))^2 / df_{Error}}$$

where  $\hat{y}_{ij}(t) = \hat{\mu}(t) + \hat{\alpha}_i(t) + \hat{\beta}_j(t) + \hat{\gamma}_{ij}(t)$  are the fitted values of model (1),  $\bar{y}(t)$  is the grand mean,  $df_{Model} = (I-1) + (J-1) + (I-1)(J-1)$ , and  $df_{Error} = \sum_{i=1}^I \sum_{j=1}^J n_{ij} - df_{Model} - 1$ . Instead, for tests on  $H_{0,A}^{\mathcal{I}}$ ,  $H_{0,B}^{\mathcal{I}}$ , and  $H_{0,AB}^{\mathcal{I}}$ , we use:

$$F_A^{\mathcal{I}} = \int_{\mathcal{I}} \sum_{i=1}^I n_{i\cdot} (\bar{y}_{i\cdot}(t) - \bar{y}(t)) / (I-1)$$

$$F_B^{\mathcal{I}} = \int_{\mathcal{I}} \sum_{j=1}^J n_{\cdot j} (\bar{y}_{\cdot j}(t) - \bar{y}(t)) / (J-1)$$

$$F_{AB}^{\mathcal{I}} = \int_{\mathcal{I}} \sum_{i=1}^I \sum_{j=1}^J (n_{ij} - (\bar{y}_{ij}(t) - \bar{y}_{i\cdot}(t) - \bar{y}_{\cdot j}(t) + \bar{y}(t))) / ((I-1)(J-1))$$

where, with the common ANOVA notation,  $\bar{y}_{i\cdot}(t) = \sum_{j=1}^J \sum_{l=1}^{n_{ij}} y_{ijl}(t) / (n_{i\cdot})$ ,  $\bar{y}_{\cdot j}(t) = \sum_{i=1}^I \sum_{l=1}^{n_{ij}} y_{ijl}(t) / (n_{\cdot j})$ , and  $\bar{y}_{ij}(t) = \sum_{l=1}^{n_{ij}} y_{ijl}(t) / n_{ij}$ .

This provides exact tests for  $H_{0,Model}^{\mathcal{I}}$ , and approximated (asymptotically exact) tests for  $H_{0,A}^{\mathcal{I}}$ ,  $H_{0,B}^{\mathcal{I}}$  and  $H_{0,AB}^{\mathcal{I}}$ . In the following, we denote with  $p_{Model}^{\mathcal{I}}$ ,  $p_A^{\mathcal{I}}$ ,  $p_B^{\mathcal{I}}$ , and  $p_{AB}^{\mathcal{I}}$  as the  $p$ -values of tests (6-9) respectively.



**Second step: computation of the adjusted  $p$ -value function.** An adjusted  $p$ -value function is computed for each test (2-5). In detail, for each  $t \in (a, b)$ , the  $p$ -value  $\tilde{p}(t)$  is computed as the maximum  $p$ -value of all interval-wise tests (6-9) on intervals containing  $t$ :

$$\tilde{p}_{Model}(t) = \sup_{\mathcal{I} \ni t} p_{Model}^{\mathcal{I}}, \quad \tilde{p}_A(t) = \sup_{\mathcal{I} \ni t} p_A^{\mathcal{I}}, \quad \tilde{p}_B(t) = \sup_{\mathcal{I} \ni t} p_B^{\mathcal{I}}, \quad \tilde{p}_{AB}(t) = \sup_{\mathcal{I} \ni t} p_{AB}^{\mathcal{I}}.$$

The adjusted  $p$ -value function  $\tilde{p}_{Model}(t)$  is provided by a control of the interval-wise error rate, while the adjusted  $p$ -value functions  $\tilde{p}_A(t)$ ,  $\tilde{p}_B(t)$ , and  $\tilde{p}_{AB}(t)$  are provided with an asymptotic control of the interval-wise error rate as defined in Pini and Vantini (2015).

**Third step: domain selection.** The intervals of the domain presenting a rejection of the null hypothesis are obtained by thresholding the corresponding adjusted  $p$ -value function at level  $\alpha$ . We select intervals presenting at least one significant effect by thresholding  $\tilde{p}_{Model}(t)$ , intervals presenting a significant effect of the  $A$  factor by thresholding  $\tilde{p}_A(t)$ , and so on.

The control of the interval-wise error rate allows controlling the probability of detecting false positive intervals, i.e., the probability of wrongly rejecting any interval. For instance, since  $\tilde{p}_{Model}(t)$  is provided by a control of the interval-wise error rate, by selecting the intervals associated with an adjusted  $p$ -value  $\tilde{p}_{Model}(t) \leq \alpha$ , given any interval in which the response is not influenced by any factor, the probability that this interval is (wrongly) selected as significant is lower than  $\alpha$ .

It is worth mentioning that, as shown by Pini and Vantini (2015), the procedure is also consistent. In detail, the probability of detecting any interval where the factors  $A$  or  $B$  have an effect on the response functions converges to one as the sample size increases.

## 2.2 Supervised profile monitoring

Once the relevant portions of a functional pattern have been selected, a supervised profile monitoring technique can be applied to detect specific changes in the corresponding domain. Such a fault-sensitized control charting approach may be coupled with traditional (unsupervised) monitoring tools in order to increase the reactivity to specific faults without losing information about other possible out-of-control events.

The proposed profile monitoring approach (Noorossana et al., 2012; Woodall et al., 2004; Colosimo et al., 2015) consists of monitoring the basis coefficients via a Hotelling's  $T^2$  control chart coupled with a control chart on the sum of the squared model residuals. Exploiting the result of the domain-selective ANOVA only the coefficients associated with the basis functions that are non-zero over the selected interval are monitored via the  $T^2$  control chart. Analogously, the model residuals are computed only within the same interval.

Assume  $M$  functional profiles,  $y_m(t)$ ,  $t \in (a, b)$ ,  $m = 1, \dots, M$  were acquired under in-control conditions to be used for control chart design (phase I). The basis expansion considered in this study consists of a cubic B-spline basis, but the methodology is applicable to any other basis. The profile approximation is such that:

$$y_m(t) = \sum_{q=1}^{Q+L-1} c_{q,j} \phi_q(t, \boldsymbol{\tau})$$

where  $Q$  is the order of the B-spline functions,  $L$  is the number of subintervals separated by  $L - 1$  interior knots,  $\boldsymbol{\tau}$  is the knot sequence  $\boldsymbol{\tau} = (\tau_1, \dots, \tau_L)'$ ,  $c_{q,m}$  are the B-spline coefficients, and  $\phi_q(t, \boldsymbol{\tau})$  are the B-spline basis functions.

Let  $\mathcal{I}$  be the interval selected by using the proposed approach and  $\phi_k^*$ ,  $k = 1, \dots, K$  the  $K$  B-spline functions that are non-zero within the interval  $\mathcal{I}$  (where  $K \leq Q + L - 1$ ). Let  $\mathbf{c}_m^* = (c_{1,m}^*, \dots, c_{K,m}^*)$  be the corresponding coefficients. The  $T^2$  statistic is then computed as follows:

$$T_m^2(\mathcal{I}) = (\mathbf{c}_m^* - \bar{\mathbf{c}}_m^*) S_c^{-1} (\mathbf{c}_m^* - \bar{\mathbf{c}}_m^*)' \quad j = 1, \dots, M$$

where  $\bar{\mathbf{c}}_m^*$  and  $S_c^{-1}$  are the sample mean and sample variance-covariance matrix of the non-zero B-spline coefficients within the interval  $\mathcal{I}$ . The “sum of prediction error” (SPE) is used as control statistic for the residual control chart:

$$SPE_m(\mathcal{I}) = \int_{\mathcal{I}} (\hat{y}_m(t) - \bar{y}_m(t))^2 dt, \quad m = 1, \dots, M$$

where  $\hat{y}_m(t)$  is the  $m$ -th signal approximated within the interval  $\mathcal{I}$  and  $\bar{y}_m(t)$  is the cross-average pattern of phase I data. The control limits of both charts are estimated as percentiles of the empirical distributions and using the Sidak correction to guarantee a family-wise type I error rate.

## 3 Simulation study

### 3.1 One-way domain-selective functional ANOVA

A simulation study is presented to investigate the suitability of the domain-selective ANOVA methodology to enhance profile monitoring performances in the presence of known local changes of the functional pattern of signal data. The results achieved by applying a one-way domain-selective ANOVA are presented, first. Additional results in the presence of a two-way ANOVA model are presented in Subsection 3.2. An in-control pattern was generated by using the following model:

$$y_m(t) = \sum_{k=1}^8 A_k g_k(t; \mu_k, \sigma_k) + \varepsilon_m(t), \quad m = 1, \dots, M; t \in (a, b) \quad (10)$$

where the functional terms  $g_k(t; \mu_k, \sigma_k)$  are normal probability density functions with parameters listed in Table 1,  $A_k \sim \mathcal{N}(10, 0.5)$  is the random amplitude term, and  $\varepsilon_m(t) \sim \mathcal{N}(0, 0.025)$ . Note that the normal probability density functions with parameters listed in Table 1 are fixed terms only used to set the functional shape of in-control profiles. On the contrary, the values  $A_k$  are random values simulated from a normal probability density function.

The simulated profiles consists of  $n = 200$  equispaced datapoints over the interval  $(a, b) = (1, 200)$ . The profiles were approximated by using a B-spline basis expansion of order 2 that consists of 200 basis functions with an equispaced knot sequence over the profile domain.

Model term ( $k$ )	$\mu_k$	$\sigma_k$
1	25	6
2	35	3
3	40	4
4	45	2
5	60	3
6	100	20
7	150	10
8	180	3

Table 1: Parameters used in the simulation model (in-control conditions)

The model (10) is used to generate a stream of independent profile data. As an example, a superimposition of  $M = 1000$  randomly generated in-control profiles and their cross-sectional average are shown in Fig. 1.

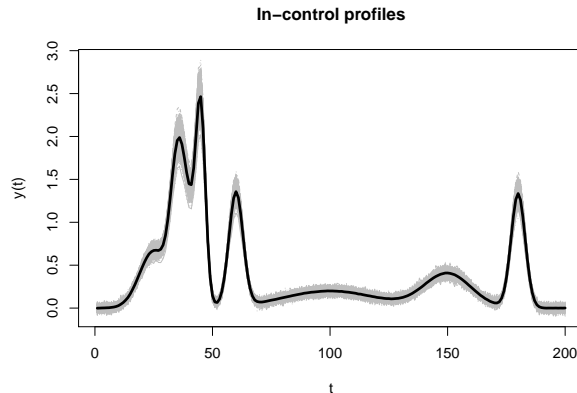


Figure 1:  $M = 1000$  randomly generated in-control profiles (grey) and their cross-sectional mean (thick black line)

The model (10) is such that closer profile locations are more correlated than locations that are far apart. Such a profile pattern has been selected as it is representative of real signal data and within-profile correlation structures in profile monitoring application. Nevertheless, future studies may be aimed at investigating either more complicated within-profile or between-profile correlation structures.

Two different scenarios for out-of-control pattern simulation were considered. Scenario 1 consists of local shape modifications of the profile, whereas Scenario 2 consists of local mean shifts. Scenario 1 is representative of out-of-control events that are hardly detected by using traditional monitoring methods based on synthetic indexes. Scenario 2 is representative of simpler deviations from an in-control pattern, although their local nature may reduce the effectiveness of traditional monitoring methods.

Each scenario comprises three different faults, referred to as Fault A, B, C in Scenario 1 and Fault D, E and F in Scenario 2. The out-of-control functional patterns were generated by using the following model:

$$y_m(t) = \sum_{k=1}^8 (\delta_{I_k} S + A_k) g_k(t; \mu_k, \delta_{II_k} \sigma_k) + \varepsilon_m(t), \quad j = 1, \dots, M; t \in (a, b) \quad (11)$$

where the shift terms  $\delta_{I_k}$  and  $\delta_{II_k}$  assume different values for different fault scenarios, as shown in Table 2, whereas  $S$  is a term that is equal to 1 for all the faults except Fault C, where it consists of a sinusoidal signal defined as  $S = \sin(t/3)$ .

Scenario	Fault	$\delta_{I_k}$	$\delta_{II_k}$	$S$
Scenario 1	A	$\delta_{I_3} = -d_I; \delta_{I_5} = d_I; \delta_{I_k} = 0$ otherwise	$\delta_{II_k} = 1 \ k = 1, \dots, 8$	1
	B	$\delta_{I_k} = 0 \ k = 1, \dots, 8$	$\delta_{II_5} = d_{II}; \delta_{II_k} = 1$ otherwise	1
	C	$\delta_{I_6} = d_I; \delta_{I_k} = 0$ otherwise	$\delta_{II_k} = 1 \ k = 1, \dots, 8$	$\sin(t/3)$
Scenario 2	D	$\delta_{I_6} = d_I; \delta_{I_k} = 0$ otherwise	$\delta_{II_k} = 1 \ k = 1, \dots, 8$	1
	E	$\delta_{I_8} = d_I; \delta_{I_k} = 0$ otherwise	$\delta_{II_k} = 1 \ k = 1, \dots, 8$	1
	F	$\delta_{I_k} = d_I \ k = 1, \dots, 5; \delta_{I_k} = 0$ otherwise	$\delta_{II_k} = 1 \ k = 1, \dots, 8$	1

Table 2: Shift parameters used in the simulation model (out-of-control conditions). The  $d_I$  values used for the simulation are summarized in Table 3

Fault A is representative of a shape modification that affects the profile portion with higher amplitude and higher local variability, with a limited effect on the cross-section average. Fault B is representative of a fault that modifies the shape of a narrow profile portion, i.e. the one corresponding to the fifth Gaussian term. Fault C consists of a superimposition of a sinusoidal term in a limited portion of the profile, representative of a distortion caused by a vibratory pattern. With regard to Scenario 2, Faults D, E and F consist of positive mean shifts of Gaussian terms. Fault D affects the profile portion where

the signal to noise ratio is lower. Fault E affects only the last Gaussian term, whereas Fault F affects the first five Gaussian terms, i.e. the portion of profile that captures the largest portion of total amplitude variability. For a visualization of the different effects of the faults, see Subsection 3.1.1.

Each simulation run consists of two sequential steps. In the first step, a single-factor experiment is simulated where the factor consists of one of aforementioned faults and its levels corresponds to its severity. During this phase, the domain-selective ANOVA methodology is applied to determine the profile portion that is significantly affected by the fault. In the second step, a dataset that comprises random realizations of both in-control and out-of-control patterns is generated to test profile monitoring performances. Profile monitoring is applied in two ways: (i) ignoring the result of the domain selection, i.e., considering the entire profile domain, and (ii) exploiting the result of the domain selection to monitor the profile only in the relevant interval. The variants (i) and (ii) are called respectively “traditional approach” and “domain-based approach” in the following.

The profile monitoring approach (Woodall et al., 2004; Noorossana et al., 2012; Colosimo et al., 2015) consists of monitoring the spline model coefficients via a Hotellings  $T^2$  control chart coupled with a control chart on the sum of the squared residuals of the spline model. In the domain-based version, the retained coefficients are those of basis functions that are non-zero over the selected interval and the model residuals are computed only over that interval. Two competitor methods were considered that are representative of monitoring methods commonly used in the industry. The first competitor is called “location control chart” (Boeing Commercial Airplane Group, Quality Assurance Department, 1998): it consists of a control envelope associated with the signal where the upper and lower control limits are  $k$  standard deviations from the in-control cross-sectional mean at each location. According to this method, an alarm is issued when at least one data point of the profile exceeds the control limits. By using Bonferroni’s correction, one can guarantee an overall false alarm rate equal to the target value. The method was applied both to the traditional implementation and the domain-based implementation.

Another competitor approach consists of estimating one (or more) synthetic indices for each profile and using it (them) to design univariate (or multivariate) control charts. In this study, the area under the curve is monitored by applying a Shewhart control chart (Montgomery, 2008). The method is referred to as “index-based control chart”. Also in this case, the area index can be computed either for the traditional implementation or the domain selection procedure. The implementation details of the two steps of the simulation study together with the major results are briefly described in Subsections 3.1.1 and 3.1.2.

### 3.1.1 Profile domain selection results

500 simulation runs were performed for each fault scenario. The first step of each simulation run consists of a single-factor experiment that involves four levels, respectively denoted by “in-control”, “out-of-control, low severity”, “out-of-control, medium severity”, and “out-of-control, high severity”. Each level was replicated five times. The severity levels associated with the parameters  $\delta_{I_k}$  and  $\delta_{II_k}$  are listed in Table 3. The selection of quite large severity levels resembles what happens in industrial practice. The injection of artificial faults in a manufacturing process usually yields macroscopic effects on the signals, whereas the observation of incipient (low severity) faults is typically troublesome and difficult to control. On the other hand, large severity levels favor the identification of the affected portion of signal profile even with a small number of factor level replicates.

Scenario	Fault	Severity
Scenario 1	A	$d_I \in \{4, 8, 12\}$
	B	$d_{II} \in \{1.5, 2.5, 4\}$
	C	$d_I \in \{5, 15, 25\}$
Scenario 2	D	$d_I \in \{4, 8, 12\}$
	E	$d_I \in \{5, 10, 15\}$
	F	$d_I \in \{4, 8, 12\}$

Table 3: Fault severity levels used for the domain-selective functional ANOVA

Figure 2 shows an example of the domain-selective functional ANOVA methodology results for one simulation run of each fault. The method clearly identifies the profile portions affected by each fault.

### 3.1.2 Profile monitoring results

Each simulation run consists of a control chart design set of  $M = 4000$  randomly generated in-control patterns and a testing set of  $N = 4000$  randomly generated patterns for each severity level of the fault. The design set is further divided into a training set of first  $M_1 = 1000$  profiles which are used to determine the sample mean and variance/covariance structure under in-control conditions, and a tuning set of last  $M_2 = 3000$  profiles, used to estimate the empirical control limits via a kernel density estimation (KDE) approach (Izenman, 1991). In this case, the control limits correspond to percentiles of the empirical distribution estimated via the so-called “plug-in” KDE methodology (Sheather and Jones, 1991; Sheather, 2004) which provides appropriate results in a wide range of applications. Without loss of generality, the in-control average run length ( $ARL_0$ ) was set to  $ARL_0 = 100$ , and the performances of the competitor monitoring schemes were compared in terms of out-of-control  $ARL$ s. The five severity levels for different faults are listed in Table 4.

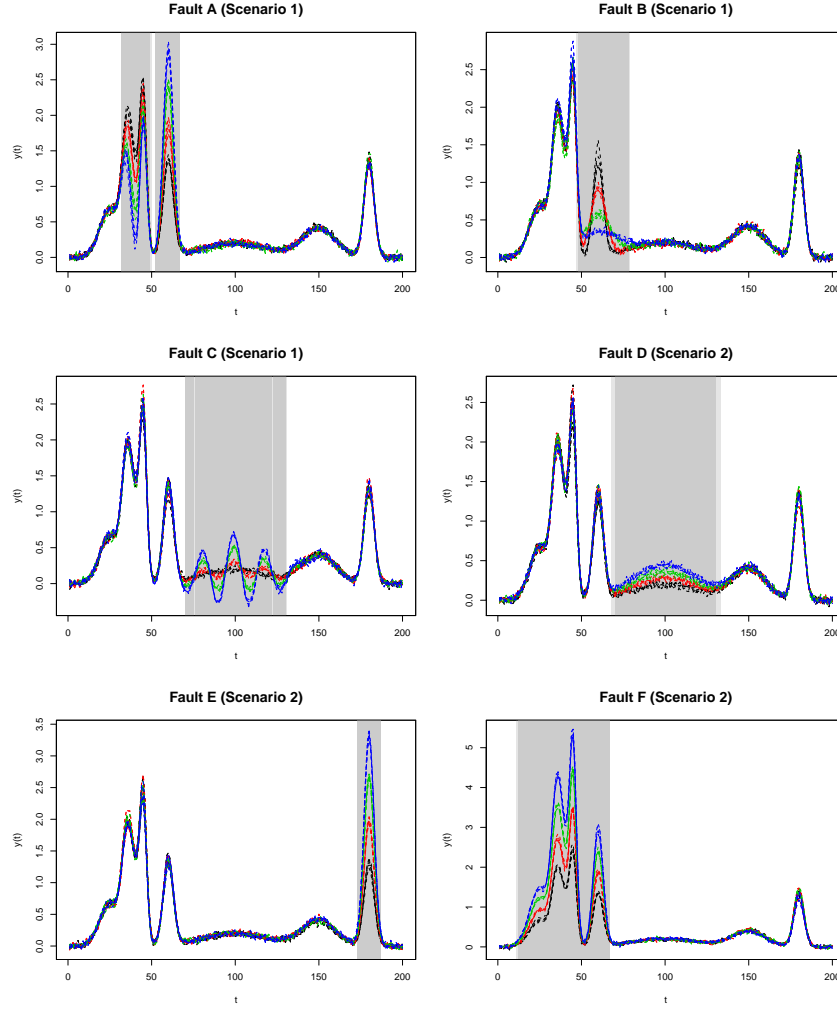


Figure 2: Domain selection results for Scenario 1 and 2; five profile replicates are shown for the in-control condition (black lines) and each severity level (red: low severity; green: medium severity; blue: high severity); the grey areas represent significant intervals at 5% and 1% levels (light and dark grey, respectively)

Scenario	Fault	Severity
Scenario 1	A	$d_I \in \{0.2, 0.5, 1, 1.5, 2\}$
	B	$d_{II} \in \{1.01, 1.025, 1.05, 1.075, 1.1\}$
	C	$d_I \in \{0.5, 1, 1.5, 2, 2.5\}$
Scenario 2	D	$d_I \in \{0.2, 0.5, 1, 1.5, 2\}$
	E	$d_I \in \{0.2, 0.5, 1, 1.5, 2\}$
	F	$d_I \in \{0.1, 0.25, 0.5, 0.75, 1\}$

Table 4: Fault severity levels used for profile monitoring testing

Notice that lower severities are considered now, because the aim consists of investigating and comparing the performances of each method when the out-of-control  $ARL$  ranges between  $ARL_0$  and one. Indeed, in the second phase of the monitoring process, we are interested in not only detecting big deviations from in-control profiles (which all methods would detect easily), but also very small deviations, which are more difficult to detect. The results of the analysis are shown in Fig. 3 and Fig. 4, for Scenario 1 (left) and Scenario 2 (right), where the  $ARL$ s and the corresponding 99% confidence intervals are depicted.

Fig. 3 shows that the index-based approach is not suitable in the presence of shape modifications like the ones in Scenario 1. With regard to the profile monitoring approach and the location control chart, the domain-based implementation always outperforms the traditional approach. The performance enhancement is achieved by exploiting only the information content that is actually relevant to the fault pattern of interest. The profile monitoring results the most effective approach in the presence of Fault B and C, whereas the location control chart is more effective in case of Fault A. This is caused by the fact that Fault A affects profile regions with high first derivative, where the narrow envelope of the location control chart is particularly sensitive to small deviations.

Fig. 4 shows that, also in Scenario 2, the domain-based approach yields a considerable enhancement of monitoring performances, with the only exception of Fault F, where profile monitoring applied to the selected interval is equivalent to profile monitoring of the entire domain. In Scenario 2, the index-based approach is suitable to monitor the profile data and it is more effective when coupled with the interval selection methodology. Nevertheless, the profile monitoring approach always outperforms the two competitors in Scenario 2.

### 3.2 Two-way domain-selective functional ANOVA

A second simulation study was performed to test the proposed approach when the domain selection depends on more than one factor. The same model (10) used in the previous case was applied to generate in-control patterns. Two faults modes are now considered: one consists of faults A, B, C, D and F previously described; the other one consists of a local trend that affects the last part of the domain. An additive model was used to simulate the superimposition of the two fault modes, which entails an additional term with respect to model (11):

$$y_m(t) = \sum_{k=1}^8 (\delta_{I_k} S + A_k) g_k(t; \mu_k, \delta_{I_k} \sigma_k) + B_m h(t) + \varepsilon_m(t), \quad j = 1, \dots, M; t \in (a, b). \quad (12)$$

The local trend term  $B_m h(t)$  is such that  $h(t) = 0, \forall t \in (a, 3b/4)$  and  $h(t) = t, \forall t \in (1 + 3b/4, b)$ . Two levels for this additional fault mode were considered, one corresponding



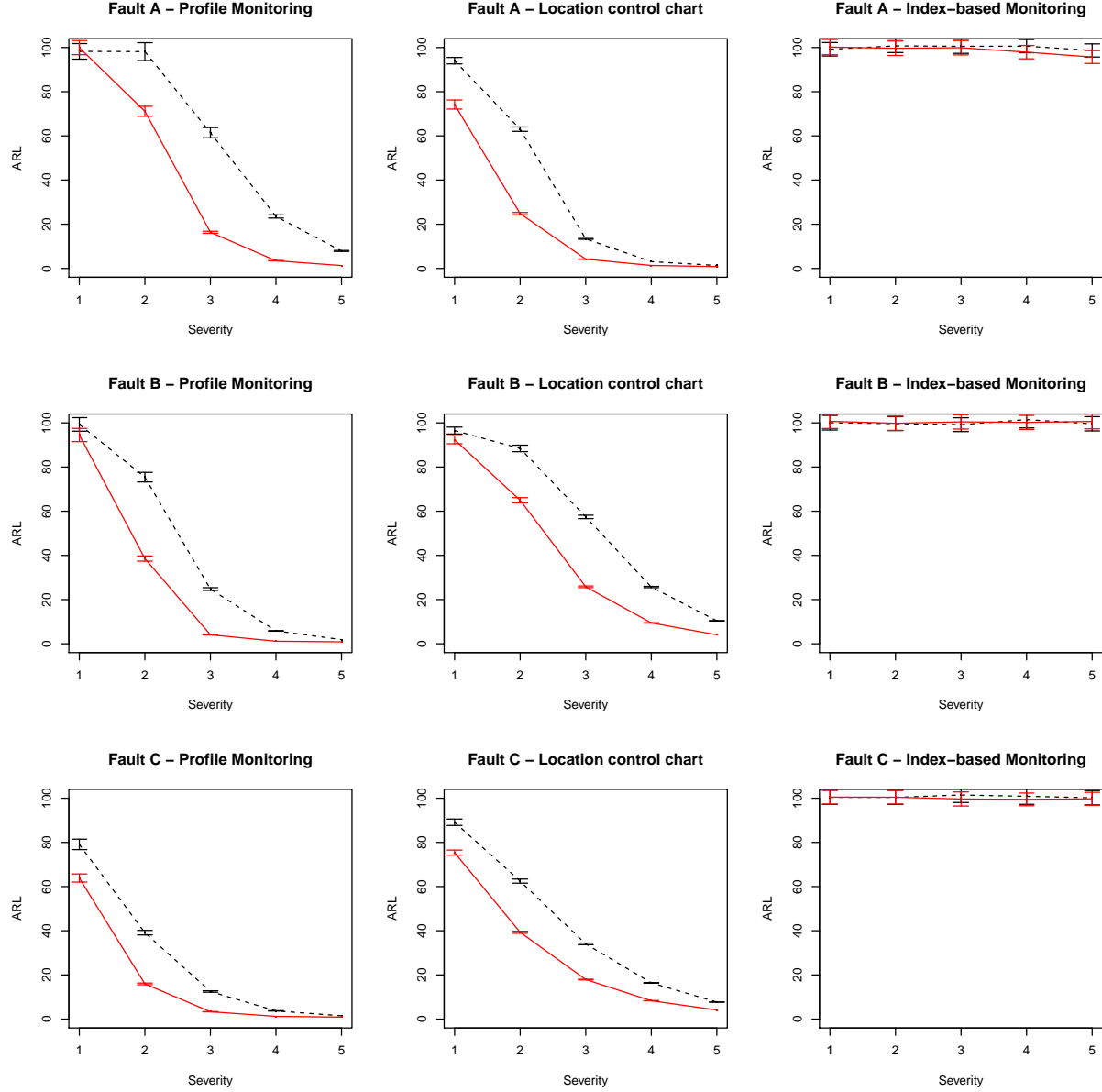


Figure 3: Profile monitoring  $ARL$  results in Scenario 1 with 99% confidence intervals (dashed black line: traditional approach; solid red line: domain-based approach)

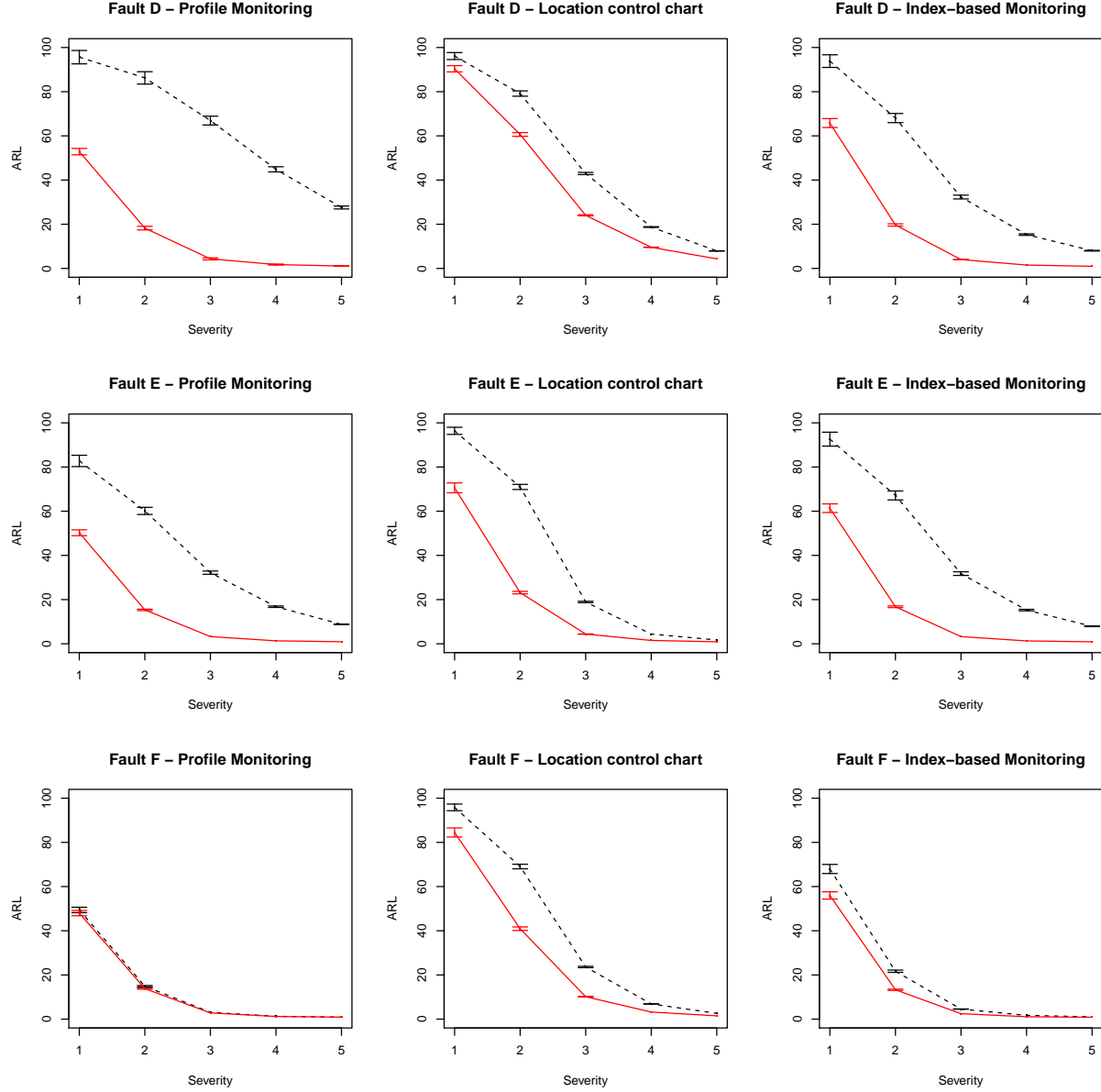


Figure 4: Profile monitoring  $ARL$  results in Scenario 2 with 99% confidence intervals (dashed black line: traditional approach; solid red line: domain-based approach)

to the absence of the local trend ( $B_m = 0, m = 1, \dots, M$ ) and one corresponding to a local trend with  $B_m \sim N(\mu_B, \sigma_B)$ , where  $\mu_B = 2.5$  and  $\sigma_B = 0.05$ . Model (12) is representative of real cases where a superimposition of effects caused by multiple faults affects the pattern of the monitored curves.

Analogously to the previous simulation study, each run consists of two sequential steps. In the first step a two-factors experiment is simulated, where the first factor consists of one of faults defined in Subsection 3.1 (four severity levels), and the second factor consists of the local trend term (two severity levels). During this phase, the two-way domain-selective ANOVA methodology is applied to determine the profile portion that is significantly affected by at least one of the two fault modes. In the second step, a dataset that comprises random realizations of both in-control and out-of-control patterns is generated to test profile monitoring performances. Note that in this study we are interested in monitoring both faults by means of the same functional data. So, the methodology is applied to determine the profile portion that is significantly affected by at least one of the two fault

A total number of 500 simulation runs was performed for each fault scenario. The first step of each run consists of a two-factors experiment where each treatment was replicated five times. Fig. 5 shows an example of the two-way domain-selective functional ANOVA methodology results for one simulation run of each superimposition of faults. Differently from Fig. 5, a double region is selected, including the portions of domain where at least one of the fault modes significantly affects the functional pattern. **test F**.

Regarding the comparison of monitoring methods, the same number of simulation runs and the same settings described in Subsection 3.1 were used. In the training set, a null severity of all the faults was applied and no local trend was added. In the testing set, a constant severity of the trend term was considered, with  $\mu_B = 0.1$  and  $\sigma_B = 0.01$ , with a varying severity of other faults. The results of the analysis are shown in Fig. 6 and Fig. 7, for Scenario 1 and Scenario 2, respectively, where the  $ARL$ s and the corresponding 99% confidence intervals are depicted.

Fig. 6 and Fig. 7 confirm the main conclusions drawn in the previous case. The superimposition of the trend term with constant severity caused a reduction of the  $ARL$  values for all the competing methods. As an example, in Scenario 1, the  $ARL$  of index-based control charts does not depend on the severity of faults A, B and C, but it is lower than  $ARL_0$  because of the trend term having constant severity. The performances of all the considered control charts improved by focusing the monitoring analysis only on the relevant portion of the domain.

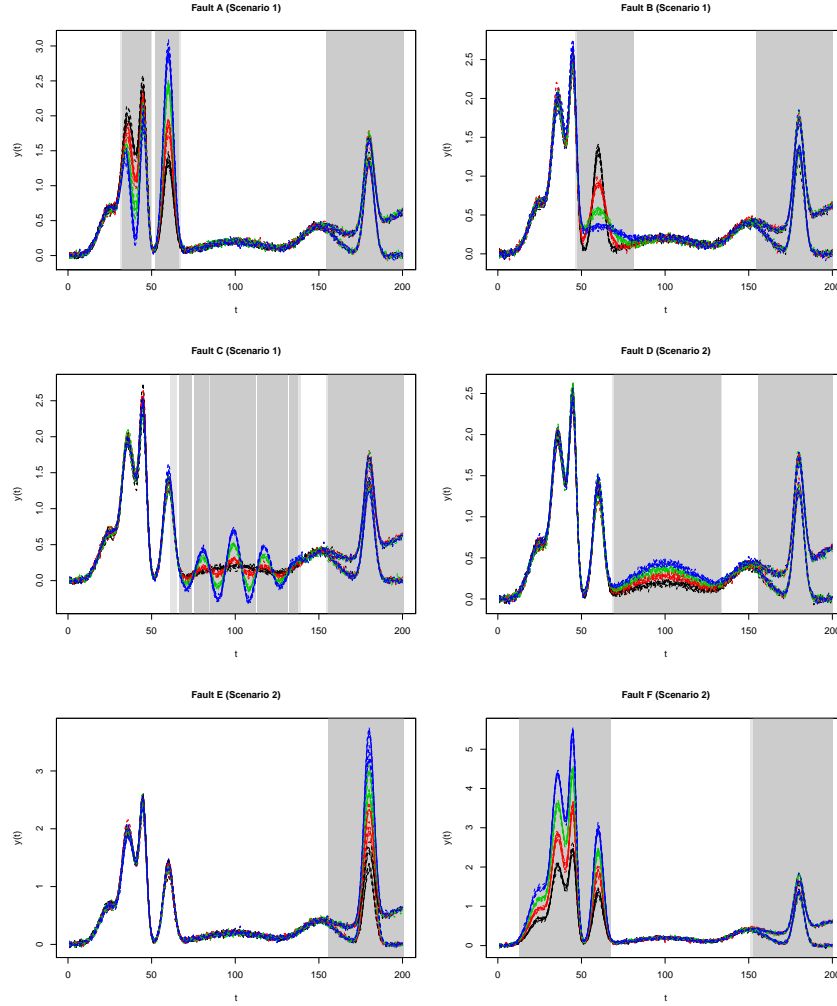


Figure 5: Domain selection results using the two-way domain-selective ANOVA model; five profile replicates are shown for each treatment; the grey areas represent significant intervals at 5% and 1% levels (light and dark grey, respectively)

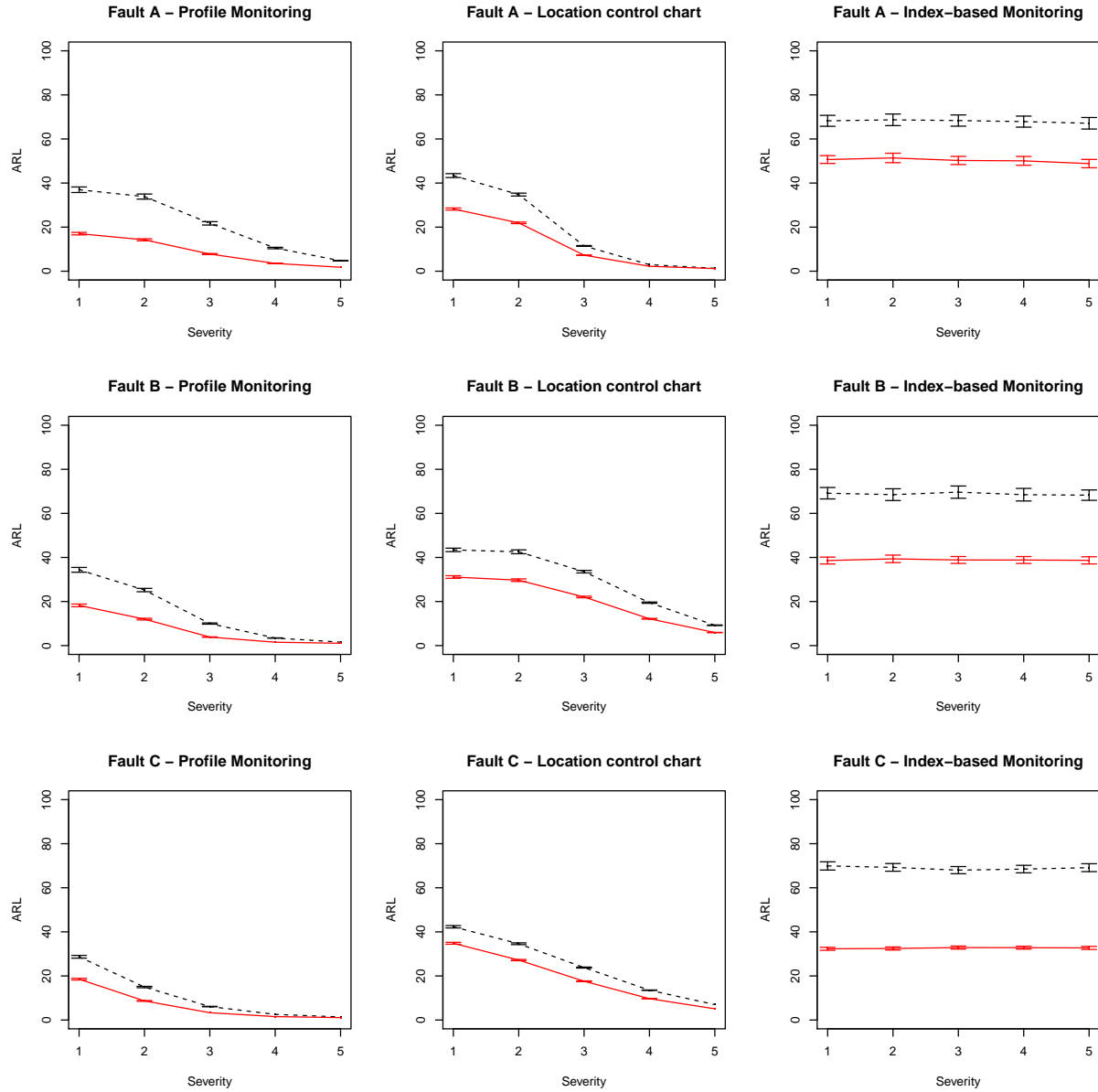


Figure 6: Profile monitoring  $ARL$  results in Scenario 1 with 99% confidence intervals (dashed black line: traditional approach; solid red line: domain-based approach) – two-way domain-selective ANOVA

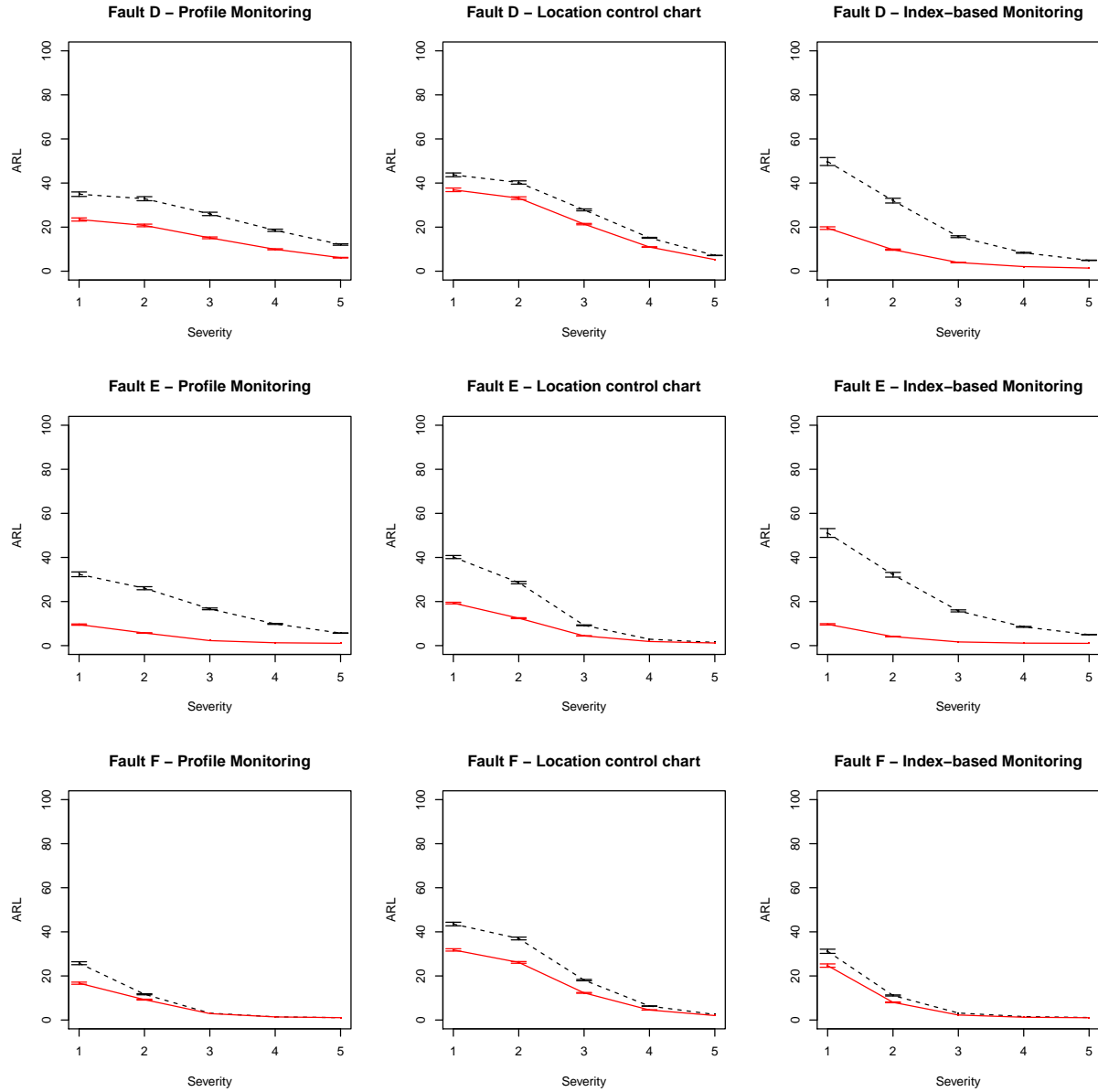


Figure 7: Profile monitoring  $ARL$  results in Scenario 2 with 99% confidence intervals (dashed black line: traditional approach; solid red line: domain-based approach) – two-way domain-selective ANOVA

## 4 Case study: process monitoring in remote laser welding

To illustrate the potential of the proposed approach, this section presents a real case study in remote laser welding. The term “remote” refers to a configuration in which the laser beam is moved along the seam with the help of a laser scanner. One of the most common applications of this process is the welding of zinc-coated steel in the lap-joint configuration (Colombo et al., 2013). However, such a configuration and the materials used many technical issues. Highly pressurized zinc vapors are often produced at the interface of the two metal sheets which may cause defects in the welded material such as inclusions and porosities. Some solutions were proposed in the literature to prevent these defects (Akhter et al., 1991; Steen et al., 2003; Daimler Chrysler AG, 2005; Schwoerer, 2008; Gu, 2010), mainly based on leaving a small gap (order of hundreds microns) between the metal sheets to facilitate the degassing. However, errors in the final gap dimension may compromise the quality of the welded material and the mechanical properties of the weld bead. Indirect monitoring of the gap between the welded surfaces therefore represents a key issue to keep the process under control and to determine the process quality without destructive off-line tests (Colombo et al., 2013).

During remote welding of zinc-coated steel in the lap-joint configuration, the optical emission of the welded material as a function of the wavelength can be used for process characterization and monitoring purposes. Specifically, we are interested in selecting the informative part of these profiles to monitor the gap between the two welded surfaces by taking into account the location in which the emission spectra are acquired.

A Through Optical Combiner Monitoring architecture (Capello et al., 2008; Colombo and Previtali, 2009, 2010) is used to monitor the laser welding. According to this technique, the monitoring of the laser emission is performed remotely. In fact, far from the work area, the optical emissions from the welding process are directly observed through the optical combiner of the fiber laser source with a spectroscope. An extensive description of the experimental welding procedure and the monitoring technology goes beyond the scope of this paper and can be found in Colombo et al. (2013).

The optical emission depends not only on the gap but also on the location in the weld seam where the spectrum is acquired. That is why, in Colombo et al. (2013), a two-way analysis of variance is performed to evaluate the effect of the gap on the emission taking into account the different locations. The former analysis is a valid instrument to assess how the emission is influenced by the gap, and the results can be used to provide an indicator to evaluate the gap remotely. However, the choice of a better indicator to evaluate the gap effect is difficult to perform since the analyzed wavelength bands are fixed a priori. Here,

we perform a domain selective functional ANOVA, according to the procedure described in Section 2 to select the wavelength bands that are affected by the gap and/or by the welding location. The selected bands can thus be used to remotely monitor the gap between the plates during the welding process.

## 4.1 Experimental procedure and data acquisition

The optical emissions were acquired for different levels of gap and location, in a repeated factorial design. Three values of gap corresponding to 100 nm, 200 nm and 300 nm were explored. For each of the analyzed gap values, three replicates were produced resulting in nine welded specimens. Interior each specimen, five emission spectra were acquired at five different locations resulting in 45 acquired spectra. The emission data are described in detail in Colombo et al. (2013).

To record the optical emission in the visible range, optical emission spectroscopy, i.e., the analysis of emitted light with high-wavelength resolution is used. The functional shape of the spectrum is then used as functional response. The laser emission  $y_{ijl}(t)$  is acquired at 703 discrete wavelengths  $t$  between 400.521 nm and 800.030 nm (where indexes  $i, j, l$  indicate the levels of gap, location and replicate, respectively). The acquired data, as well as the three means, corresponding to the three different values of the gap, are represented in Figure 8. In the figure, the curves of each color correspond to the 15 functional emissions (five locations and three replicates) within each gap level.

Note that in the explored wavelength range, it is possible to distinguish between three different emission ranges:

- between 400 nm and 530 nm, it is observed the emission related to the electronic transition, i.e., the plasma emission (light blue area of Figure 8);
- around 535 nm we observe a strong emission line, corresponding to the laser emission (light green area of Figure 8);
- above 540 nm we observe the emission due to the thermal black-body radiation, i.e. the thermal emission (light red area of Figure 8).

## 4.2 Results

The emission functions  $y_{ijl}(t)$  ( $i = 1, \dots, 3, j = 1, \dots, 5, l = 1, \dots, 3$ ) are modeled according to model (1), where  $t$  is the wavelength,  $\alpha_i(t)$  is the gap functional effect,  $\beta_j(t)$  is the location functional effect,  $\gamma_{ij}(t)$  is the interaction functional effect, and  $\epsilon_{ijl}(t)$  is the functional error term.



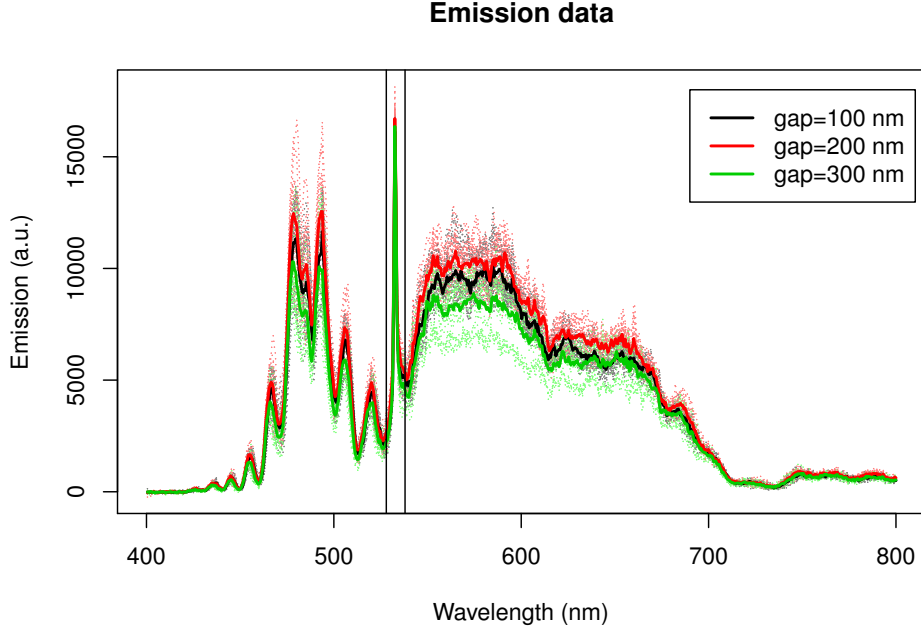


Figure 8: Emission data captured in the factorial laser welding experiment (dashed lines), colored according to the three different gaps; and means of the three groups, corresponding to the three different gaps (solid lines). The vertical lines divide the figure along the abscissa into the plasma (left), laser (middle), and thermal (right) emissions.

We applied the domain-selective functional two-way ANOVA described in Section 2 to test the null model  $H_{0,Model}$  (2), the gap effect  $H_{0,Gap} = H_{0,A}$  (3), the location effect  $H_{0,Loc} = H_{0,B}$  (4), and the interaction effect  $H_{0,GapLoc} = H_{0,AB}$  (5). Since the original data are discrete evaluations of the curves, to obtain the functional data set we first performed a smoothing of the 703 discrete data points on a dense piece-wise linear B-spline basis characterized by 200 knots. The functional data are reported in the right panels of Figure 10. A robustness analysis with respect to the number of knots of the expansion is reported in the Appendix. The test statistics of tests on intervals were approximated through a rectangle integration method. Thanks to the continuity of test statistics with respect to the extremes of integration, the adjusted  $p$ -value functions were approximated through a finite family of tests over a fine discrete grid of 703 points (i.e., the maximal resolution of the monitoring instrument). The permutation  $p$ -values were estimated by means of a Conditional Monte Carlo algorithm based on 1000 iterations.

The results of the test for the interaction term  $\gamma_{ij}(t)$  are reported in Figure 9. In detail, the left panel shows the adjusted  $p$ -value function for the test of  $H_{0,GapLoc}$ , and the right panel shows the emission data obtained after the B-spline smoothing. Since the interaction

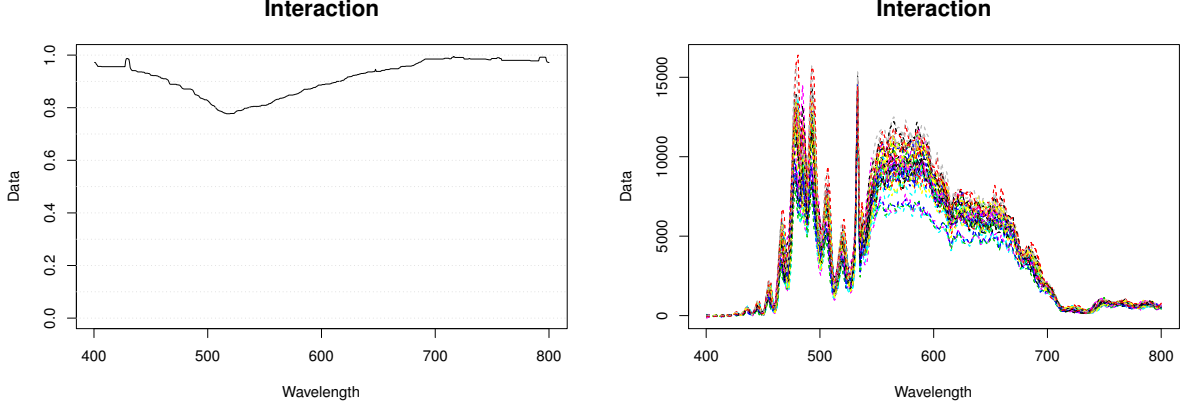


Figure 9: Left: adjusted  $p$ -value function for the tests on  $\tilde{H}_{0,GapLoc}$ . Right: emission data colored according to gap and location levels.

effect is not significant (i.e., the adjusted  $p$ -value function presents high values along all the wavelength domain), this term was removed from the model, and the following additive functional ANOVA model was tested :

$$y_{ijl}(t) = \mu(t) + \alpha_i(t) + \beta_j(t) + \epsilon_{ijl}(t), \quad \forall t \in (a, b). \quad (13)$$

In the following, we describe the results of the tests on the additive model (13). Note that, in this case, the test of the null model becomes:

$$\begin{cases} \tilde{H}_{0,Model} & : \alpha_i(t) = \beta_j(t) = 0, \forall i = 1, \dots, 3; j = 1, \dots, 5; t \in (400.521, 800.030); \\ \tilde{H}_{1,Model} & : (\tilde{H}_{0,Model})^C. \end{cases}$$

Figure 10 reports the results of the additive two-way functional ANOVA of emission data. In particular, the left panels report the adjusted  $p$ -value functions for each test. In detail, on the top panel, we report the adjusted  $p$ -value functions of  $\tilde{H}_{0,Model}$ , on the middle panel the adjusted  $p$ -value functions of  $H_{0,Gap}$  and on the bottom panel the adjusted  $p$ -value functions of  $H_{0,Loc}$ . For ease of visualization of the test results, the right panels of the figure report the emission data and the significant intervals detected at 5% and 1% levels (areas colored in light and dark grey, respectively) for the three tests. Data are colored in the three panels according to the corresponding tests: on the top panel data are colored differently according to the different levels of both gap and location; on the middle panel data are colored according to the different levels of gap; on the bottom panel data are colored according to the different levels of location.

Focusing on the test of  $\tilde{H}_{0,Glob}$  (i.e., top panels of Figure 10), a significant effect of at least one factor among gap and location was found in nearly the entire wavelength domain.

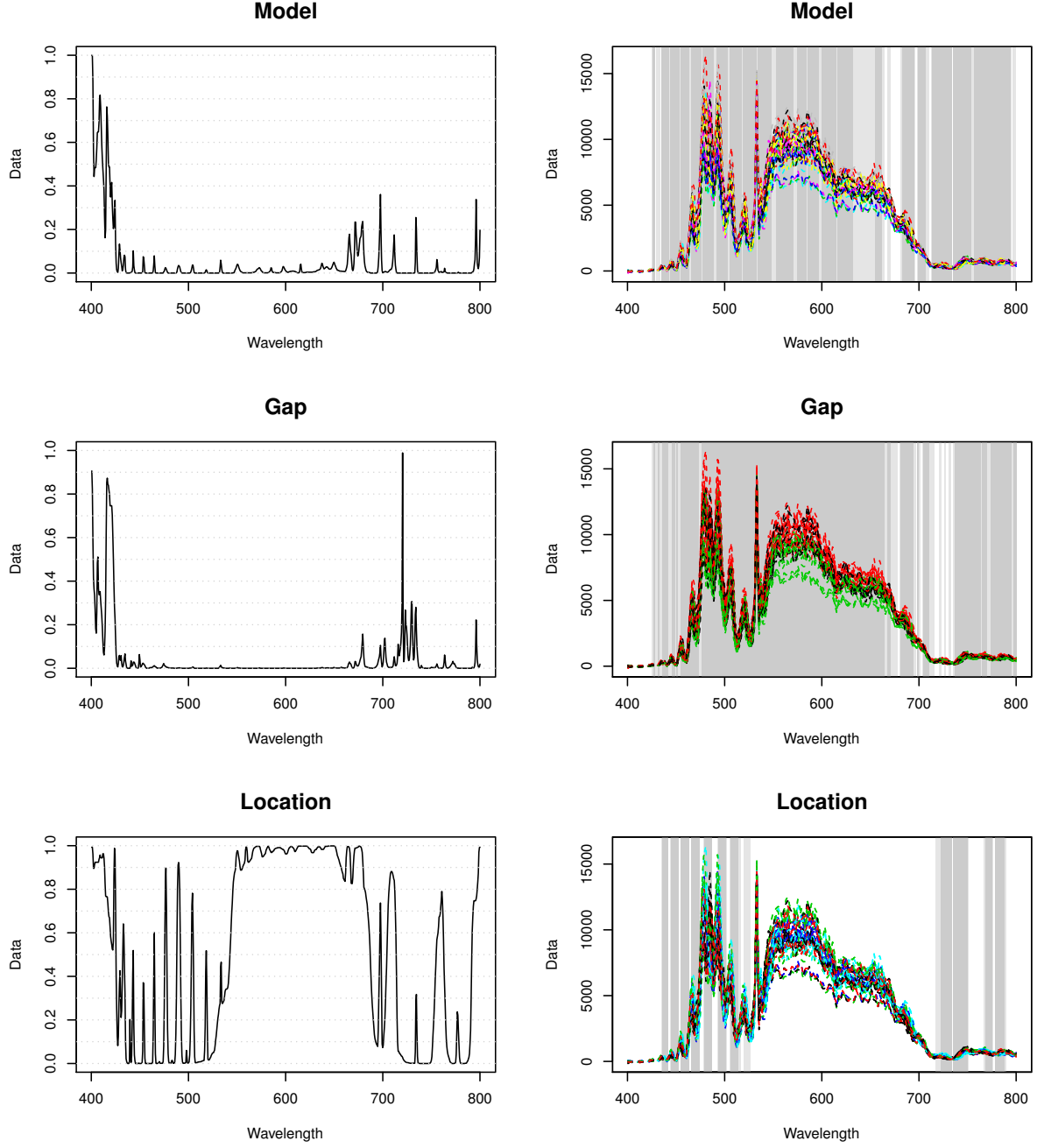


Figure 10: Left: adjusted  $p$ -value functions for the tests on  $\tilde{H}_{0,Model}$  (top),  $H_{0,Gap}$  (middle) and  $H_{0,Loc}$  (bottom). Right: emission data colored according to gap and location levels (top), gap levels (middle) and location levels (bottom). The gray areas represent significant intervals at 5% and 1% levels (light and dark grey, respectively)

This result suggests that, as expected, the welding conditions have a significant effect on the spectrum for all three emission ranges (plasma, laser, and thermal). The gap has a significant effect in most of the wavelength domain (i.e., test of  $H_{0,Gap}$ , middle panels of Figure 10), suggesting that, consistent with previous results, the emission is significantly influenced by the gap on all three emission ranges. The location has a significant effect mostly in the plasma emission range (i.e., test of  $H_{0,Loc}$ , bottom panels of Figure 10). This suggests that plasma emission is influenced by the location.

The procedure described in this paper improves the results found by Colombo et al. (2013) by precisely locating the wavelength bands associated to significant effects of the two factors. The proposed method allowed the detection of a band (i.e., the band  $t \in (547 \text{ nm}, 681 \text{ nm})$  corresponding approximately to thermal emission) in which the gap effect is significant and the location one is not. This suggests the use of emission data on this band to monitor the gap between the plates during the welding process regardless of the welding location. This yields two major benefits. On one hand, it allows implementing a more effective profile monitoring tool via a supervised control chart design phase as shown in previous sections. On the other hand, it provides useful information to develop a novel device for remote monitoring of the gap between the welded surfaces that allows analysing the phenomenon only in the relevant wavelength domain which is insensitive to location changes.

Future studies will be aimed at testing the presented approach in the presence of real fault states. Another interesting future challenge posed by this data analysis consists of introducing the gap in the functional model as a numeric explanatory variable, instead of a factor. Since the effect of the gap on the emission spectra is observed to be not monotonic, to perform this analysis, it is key to study its effect, and add the gap in the model in a non-linear way.

## 5 Conclusions

We proposed a methodology that can be applied to enhance profile monitoring performances in the presence of known fault scenarios. The method is specifically though for signal-based profile monitoring applications, where the quality of the process can be automatically assessed during the process itself via in-situ gathered data. Traditional control charts are general-purpose monitoring tools that are able to detect any change from an in-control state by issuing an alarm. The control chart design phase can therefore be regarded as an unsupervised learning procedure as no information about the out-of-control states to be detected is used. However, in many industrial applications, fault changes may have different impacts on the process performance. This motivates the use of supervised

approaches, where the term “supervised” denotes the use of out-of-control information for control chart design. Incorporating a priori knowledge about a fault signature, when available, into the design phase is suitable to develop fault-sensitized SPC schemes that can considerably increase fault detection power. In the framework of profile monitoring applications, a fault-sensitized control chart can be developed by monitoring only the portion of the functional domain where the effects of the fault are significant. To this aim, a two-step methodology is proposed. In the first step, a domain-selective functional ANOVA is performed to study the effects of one or more underlying factors on the output functions. This selection is performed by extending the interval-wise testing procedure (Pini and Vantini, 2015) to the case of multi-way ANOVA framework. The second step consists of monitoring the functional pattern only within the previously selected interval. The resulting control chart can possibly be used to supplement traditional charts, in order to combine general purpose (unsupervised) and fault-sensitized (supervised) monitoring tools. We presented a simulation study to investigate the suitability of the domain-selective functional ANOVA to enhance profile monitoring performances. In the simulation, out-of-control profiles presenting local changes of the functional pattern were simulated, and the interval-wise testing methodology was used to select the portion of the domain presenting a significant deviation from in-control patterns. Then, different profile monitoring control charts were tested and compared to highlight the benefits of the proposed approach with respect to monitoring the entire domain. The simulation study showed that, in all simulated scenarios, the proposed methodology outperformed the traditional approach, confirming the potential of a supervised design phase.

The proposed methodology was eventually applied to a real case study in remote laser welding. The aim of this study was to monitor the gap between two welded plates by observing the emission spectra of the welded material. We applied the domain-selective functional two-way ANOVA to study the effects of the gap on the output functions, by taking into account the different locations at which the emission was registered. The final result of this analysis is the selection of a wavelength band (i.e., the band  $t \in (547 \text{ nm}, 681 \text{ nm})$  corresponding to the thermal emission), in which the emission is significantly influenced by the gap and not by the location. This suggests to directly record the emission data on this band to monitor the gap between the plates during the welding process at any possible location. This result might also be used to develop a novel device for remote monitoring of the gap between the welded surfaces that allows analysing the phenomenon only in the relevant wavelength domain. The robustness of this result with respect to the number of knots  $p$  of the B-spline basis expansion employed to smooth the data is discussed in the Appendix. Even though the results of this robustness study showed that the number of knots is not a crucial parameter, it is of course of major interest for future research to

explore the trade-off, in terms of power of the procedure, as  $p$  increases. From the point of view of the application, instead, the results obtained in the analysis of laser spectra suggest to enrich the data set to further investigate the effect of the interaction, and to introduce the gap in the functional model as a numeric explanatory variable associated with a non-linear effect.

## References

- Abramovich, F. and C. Angelini (2006). Testing in mixed-effects fanova models. *J. Statist. Plann. Inference* 136(12), 4326–4348.
- Akhter, R., W. M. Steen, and K. G. Watkins (1991). Welding zinc-coated steel with a laser and the properties of the weldment. *J. Laser Appl.* 3(2), 9–20.
- Antoniadis, A. and T. Sapatinas (2007). Estimation and inference in functional mixed-effects models. *Comput. Statist. Data Anal.* 51(10), 4793–4813.
- Basseville, M. (1988). Detecting changes in signals and systemsa survey. *Automatica* 24(3), 309–326.
- Boeing Commercial Airplane Group, Quality Assurance Department (1998). Advanced quality system tools, aqs d1-9000-1. <http://www.boeingsuppliers.com/supplier/d1-9000-1.pdf>.
- Box, G. E. P. and A. Luceno (2011). *Statistical Control by Monitoring and Feedback Adjustment*. John Wiley & Sons, New York.
- Box, G. E. P. and J. Ramirez (1992). Cumulative score charts. *Quality and Reliability Engineering International* 8(1), 17–27.
- Capello, E., D. Colombo, and B. Previtali (2008). Monitoring through the optical combiner in fibre laser welding. In *ICALEO 2008 Congress proceedings*, pp. 75–84.
- Colombo, D., B. M. Colosimo, and B. Previtali (2013). Comparison of methods for data analysis in the remote monitoring of remote laser welding. *Opt. Laser. Eng.* 51(1), 34–46.
- Colombo, D. and B. Previtali (2009). Fiber laser welding of titanium alloys and its monitoring through the optical combiner. In *ICALEO 2009 Congress proceedings*, pp. 620–629.
- Colombo, D. and B. Previtali (2010). Through optical combiner monitoring of fiber laser processes. *Int. J. Mater. Form.* 3(1), 1123–1126.

- Colosimo, B. M., M. Meneses, and Q. Semeraro (2015). On the effectiveness of profile monitoring to enhance functional performance of particleboards. *Quality and Reliability Engineering International* 31(8), 1655–1674.
- Cuesta-Albertos, J. A. and M. Febrero-Bande (2010). A simple multiway anova for functional data. *TEST* 19(3), 537–557.
- Cuevas, A., M. Febrero, and R. Fraiman (2004). An anova test for functional data. *Comput. Statist. Data Anal.* 47(1), 111–122.
- Daimler Chrysler AG (2005). Patent no. DE10241593.
- Freedman, D. and D. Lane (1983). A nonstochastic interpretation of reported significance levels. *J. Bus. Econ. Stat.* 1(4), 292–298.
- Goldsmith, J. and T. Kitago (2016). Assessing systematic effects of stroke on motor control by using hierarchical function-on-scalar regression. *Journal of the Royal Statistical Society: Series C (Applied Statistics)* 65(2), 215–236.
- Gu, H. (2010). Laser lap welding of zinc coated steel sheet with laser-dimple technology. *J. Laser Appl.* 22(3), 87–91.
- Izenman, A. J. (1991). Review papers: recent developments in nonparametric density estimation. *Journal of the American Statistical Association* 86(413), 205–224.
- Lai, T. L. (1995). Sequential changepoint detection in quality control and dynamical systems. *Journal of the Royal Statistical Society. Series B (Methodological)*, 613–658.
- Lorden, G. (1971). Procedures for reacting to a change in distribution. *The Annals of Mathematical Statistics*, 1897–1908.
- Montgomery, D. C. (2008). *Introduction to statistical quality control*. John Wiley & Sons.
- Nembhard, H. (2006). Cuscore statistics: Directed process monitoring for early problem detection. In *Springer Handbook of Engineering Statistics*, pp. 249–261. Springer.
- Noorossana, R., A. Saghaei, and A. Amiri (2012). *Statistical analysis of profile monitoring*. John Wiley & Sons, New York.
- Pini, A. and S. Vantini (2015). Interval-wise testing for functional data. Technical Report 30/2015, MOX, Politecnico di Milano.

- Pomann, G. M., A. M. Staicu, and S. Ghosh (2016). A two-sample distribution-free test for functional data with application to a diffusion tensor imaging study of multiple sclerosis. *Journal of the Royal Statistical Society: Series C (Applied Statistics)*.
- R Core Team (2012). *R: a language and environment for statistical computing*. Vienna, Austria: R Foundation for Statistical Computing. ISBN 3-900051-07-0.
- Runger, G. C. and M. C. Testik (2003). Control charts for monitoring fault signatures: Cuscore versus glr. *Quality and Reliability Engineering International* 19(4), 387–396.
- Schwoerer, T. (2008). Robot-guided remote laser scanner welding for highly-productive welding applications. In *ICALEO 2008 Congress proceedings*, pp. 392–398.
- Sheather, S. J. (2004). Density estimation. *Statistical Science* 19(4), 588–597.
- Sheather, S. J. and M. C. Jones (1991). A reliable data-based bandwidth selection method for kernel density estimation. *Journal of the Royal Statistical Society. Series B (Methodological)*, 683–690.
- Shu, L., D. W. Apley, and F. Tsung (2002). Autocorrelated process monitoring using triggered cuscore charts. *Quality and Reliability Engineering International* 18(5), 411–421.
- Steen, W. M., J. Mazumder, and K. G. Watkins (2003). *Laser material processing*. Springer.
- Woodall, W. H., D. J. Spitzner, D. C. Montgomery, and S. Gupta (2004). Using control charts to monitor process and product quality profiles. *Journal of Quality Technology* 36(3), 309–320.
- Zhang, Y., Z. He, L. Shan, and M. Zhang (2014). Directed control charts for detecting the shape changes from linear profiles to quadratic profiles. *International Journal of Production Research* 52(11), 3417–3430.
- Zhang, Y., Z. He, M. Zhang, and Q. Wang (2015). A score-test-based ewma control chart for detecting prespecified quadratic changes in linear profiles. *Quality and Reliability Engineering International*.



## Appendix. Robustness analysis

To investigate the robustness of the results with respect to the number of knots of the B-spline expansion, we performed the test by varying this parameter. We considered different cases based on B-splines expansions with a different number of knots. In particular, we started from the analysis reported in Section 4 based on 200 knots and tried to double or halve the number of knots. Finally, we also tried the maximum possible resolution (i.e., 703 knots).

The test on the interaction  $H_{0,GapLoc}$  is not significant in all cases. Hence, the comparison is made on the additive model without interaction (13). The results of the tests are reported in Figure 11. Similarly in the right panels of Figure 10, the results of the tests of  $\tilde{H}_{0,Model}$ ,  $H_{0,Gap}$  and  $H_{0,Loc}$  at 1% and 5% levels are represented by means of the gray bands below each graphic. In Figure 11, The axis on the left indicates the number of knots used for the B-spline basis expansion, i.e., 100, 200, 400, and 703 knots corresponding to length of B-spline supports of 8, 4, 2, and 1.14 nm.

This further analysis shows that the results are robust with respect to the number of knots. Both the test on the null model  $\tilde{H}_{0,Model}$  and the test on the gap  $H_{0,Gap}$  report significant differences in most of the wavelength domain. In particular, the gap has a significant effect on all three emission ranges. On the other hand, the effect of the location is significant mostly on the plasma emission.

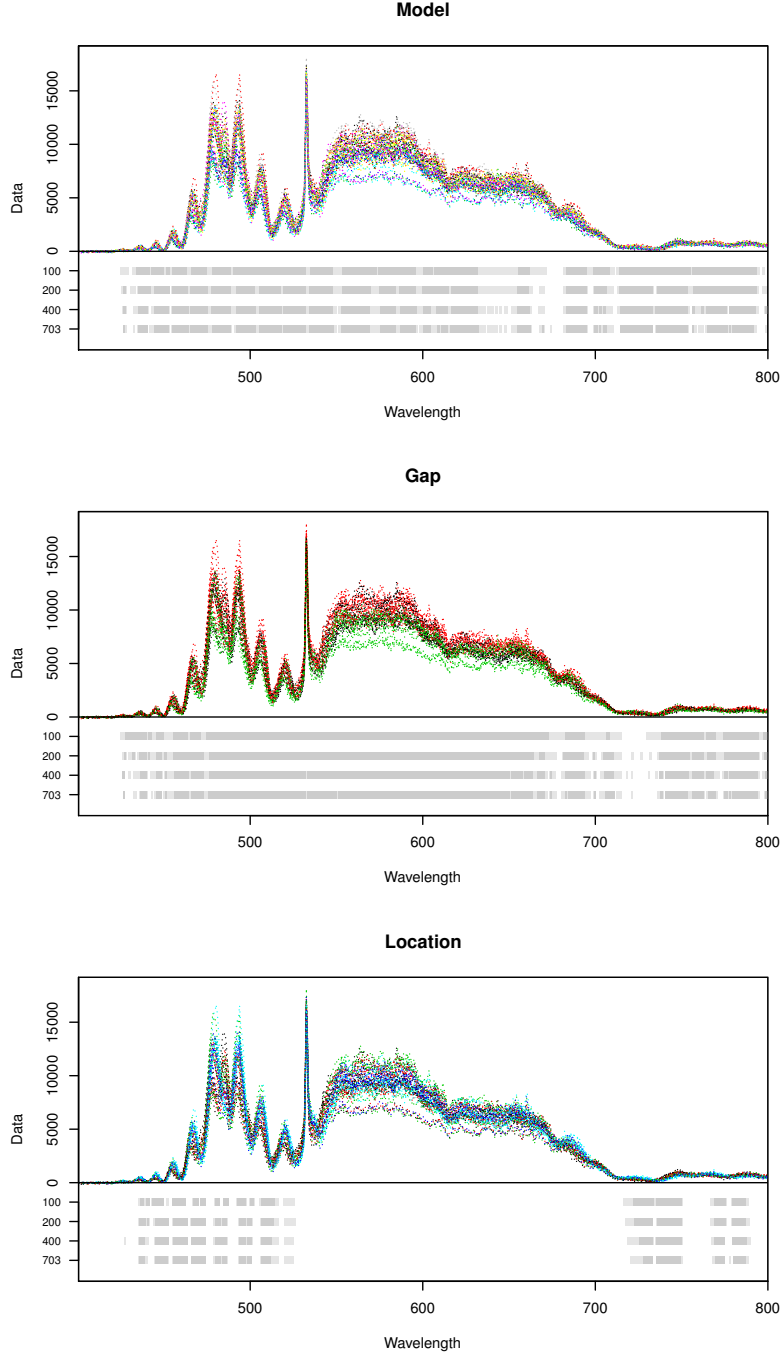


Figure 11: Emission data colored according to gap and location levels (top), gap levels (middle) and location levels (bottom). The gray bands below each graphic represent the results of tests on  $\tilde{H}_{0,Model}$ ,  $H_{0,Gap}$  and  $H_{0,Loc}$ , resp., varying the number of knots, at 5% and 1% levels (light and dark grey, resp.)